

Phase Diagram of Mg Insertion into Chevrel Phases, $Mg_xMo_6T_8$ (T = S, Se). 3. The Crystal Structure of Triclinic $Mg_2Mo_6Se_8$

E. Levi,^{*,†} A. Mitelman,[†] O. Isnard,^{‡,§} M. Brunelli,[¶] and D. Aurbach^{*,†}

Department of Chemistry, Bar-Ilan University, Ramat-Gan, Israel 52900, Institut Néel, CNRS, associé à l'Université de Grenoble J. Fourier, BP166X, 38042 Grenoble cedex 9, France, Institut Laue Langevin, BP 156 X, 38042 Grenoble cedex 9, France, and ESRF, 6 rue Jules Horowitz, BP 220, F-38043 Grenoble cedex, France

Received August 22, 2007

This series of papers is devoted to unique cathode materials for Mg batteries, $Mg_xMo_6T_8$ (T = S, Se, x = 1 and 2) Chevrel phases (CPs). In this part, a combination of neutron and high-resolution synchrotron X-ray diffractions was used to study the crystal structure of $Mg_2Mo_6Se_8$, which is triclinic at room temperature (space group $P\bar{1}$, $a = 6.868$ Å, $b = 6.921$ Å, $c = 6.880$ Å, $\alpha = 93.00^\circ$, $\beta = 94.40^\circ$, $\gamma = 96.22^\circ$). In contrast to other members of the $Mg_xMo_6T_8$ family, this compound does not follow the classic scheme of successive cation insertion into so-called inner and outer sites: Both the Mg^{2+} ions per formula are located in the tetrahedral sites of the outer ring. This surprising cation location, predicted previously for Mg-containing CPs by ab initio calculations, provides the uniform distribution of the cation charge in the triclinic structure, which is similar to that of rhombohedral CPs. A mapping of the cation sites was widely used to demonstrate the variety of cation arrangement in CPs and the factors affecting this arrangement, as well as to clarify the origin of the exceptionally high mobility of the Mg^{2+} ions in $Mg_2Mo_6Se_8$.

Introduction

Chevrel phases (CPs), $M_xMo_6T_8$ (M = metal, T = S, Se, Te), are an important class of materials with unusual physical properties.^{1–4} We are interested in CPs as unique cathodes for rechargeable Mg batteries, where the ability of the host to insert fast and reversibly multivalent cations is a crucial parameter for their function.^{5–7} Thus, our efforts were devoted to study the phase diagram of Mg insertion into

Mo_6T_8 (T = S, Se), especially the crystal structure of the intercalation compounds and its influence on the cation mobility in the hosts.^{8–10}

In spite of the basic similarity of the crystal structure of CPs as a stacking of Mo_6T_8 blocks, these materials present a surprising variety of cation arrangements in the pseudocubic cavities between the blocks (each block is composed of an octahedral cluster of molybdenum atoms inside a cube of 8 T anions).^{1,2,9–20} The cation distribution is closely related

* E-mail: elenal@mail.biu.ac.il.

† Bar-Ilan University.

‡ Université de Grenoble J. Fourier.

§ Institut Laue Langevin.

¶ ESRF.

- (1) *Topics in Current Physics: Superconductivity in Ternary Compounds I*; Fisher, Ø., Maple, M. B., Eds.; Springer-Verlag: Berlin, 1982.
- (2) Yvon, K. In *Current Topics in Material Science*; Kaldis, E., Ed.; Elsevier: North-Holland, Amsterdam, 1979; Vol. 3.
- (3) Nunes, R. W.; Mazin, I. I.; Sigh, D. *J. Phys. Rev. B* **1999**, *59*, 7969.
- (4) Benson, J. W.; Schrader, G. L.; Angelici, R. J. *J. Mol. Catal. A: Chem.* **1995**, *96*, 283.
- (5) Aurbach, D.; Lu, Z.; Schechter, A.; Gofer, Y.; Gizbar, H.; Turgeman, R.; Cohen, Y.; Moskovich, M.; Levi, E. *Nature* **2000**, *407*, 724.
- (6) Aurbach, D.; Gofer, Y.; Lu, Z.; Schechter, A.; Chusid, O.; Gizbar, H.; Cohen, Y.; Ashkenazi, V.; Moskovich, M.; Turgeman, R.; Levi, E. *J. Power Sources* **2001**, *97*, 28.
- (7) Aurbach, D.; Weissman, I.; Gofer, Y.; Levi, E. *Chem. Rec.* **2003**, *3*, 61.

- (8) Lancry, E.; Levi, E.; Gofer, Y.; Levi, M.; Salitra, G.; Aurbach, D. *Chem. Mater.* **2004**, *16*, 2832.
- (9) Levi, E.; Lancry, E.; Mitelman, A.; Aurbach, D.; Isnard, O.; Djurado, D. *Chem. Mater.* **2006**, *18*, 3705.
- (10) Levi, E.; Lancry, E.; Mitelman, A.; Aurbach, D.; Ceder, G.; Morgan, D.; Isnard, O. *Chem. Mater.* **2006**, *18*, 5492.
- (11) Bars, O.; GuilleVIC, J.; Grandjean, D. *J. Solid State Chem.* **1973**, *6*, 335.
- (12) Yvon, K.; Paoli, A.; Flukiger, R.; Chevrel, R. *Acta Crystallogr.* **1977**, *B33*, 3066.
- (13) Yvon, K.; Baillif, R.; Flukiger, R. *Acta Crystallogr.* **1979**, *B35*, 2859.
- (14) Yvon, K.; Chevrel, R.; Sergent, M. *Acta Crystallogr.* **1980**, *B36*, 685.
- (15) Hoenle, W.; Yvon, K. *J. Solid State Chem.* **1987**, *70*, 235.
- (16) Harbrecht, B.; Mahne, S. *J. Alloys Compd.* **1992**, *178*, 467.
- (17) Roche, C.; Chevrel, R.; Jenny, A.; Pecheur, P.; Scherrer, H.; Scherrer, S. *Phys. Rev. B* **1999**, *60*, 16442.
- (18) Belin, S.; Chevrel, R.; Sergent, M. *J. Solid State Chem.* **2000**, *155*, 250.

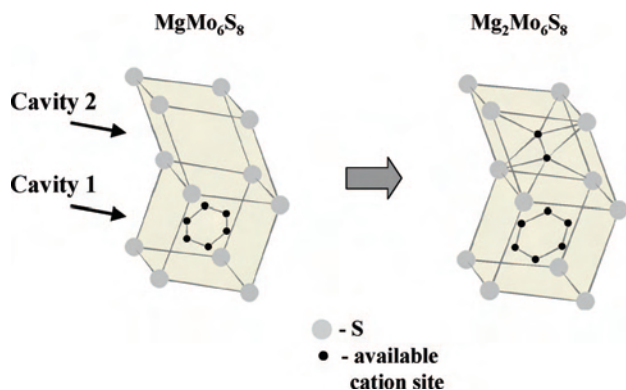
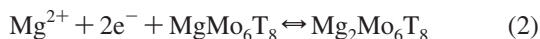
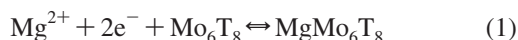


Figure 1. The cation distribution in R-Mg_xMo₆S₈ ($x = 1$ and 2).

to the CPs' symmetry, which may be rhombohedral (R) or triclinic (T).^{1,2,9–21} In the previous parts,^{9,10} it was shown that the Mg insertion into Mo₆T₈ occurs in two stages:



The sulfides at ambient temperature crystallize in rhombohedral symmetry. Their crystal structure¹⁰ is similar to that of classic CPs with small cations (Figure 1).^{1,2} In MgMo₆S₈, a single Mg²⁺ cation per formula unit is randomly distributed between six inner tetrahedral sites in cavity 1 with low potential energy. Such cation distribution and the small distances between the inner sites result in partial Mg trapping, evident during Mg deinsertion.^{8–10} Mg₂Mo₆S₈ retains the same location of the first cation, while the second cation occupies one of the six outer tetrahedral sites, which are located in six adjacent cavities 2. The assemblies of these sites, connected to each other by a $\bar{3}$ symmetry axis, are also known as inner and outer rings. Mg transport in the latter compound is fast because it is promoted by repulsion between two Mg²⁺ cations.^{8–10}

In contrast to the sulfides, the selenides are triclinic at ambient temperature. The crystal structure of MgMo₆Se₈⁹ can be basically related to the Fe₂Mo₆S₈-type:¹⁴ In both compounds, the six tetrahedra, which form cavity 1 in rhombohedral CPs, degenerate to a combination of two square pyramids and two tetrahedra⁹ (each pair of the sites are connected to each other by an inversion point, $\bar{1}$, in the center of cavity 1). The cations occupy the former sites with coordination number (CN) equal to 5, but their distribution in these two compounds is not really the same: In Fe₂Mo₆S₈, two Fe²⁺ cations form a pair with metal–metal interactions, while in MgMo₆Se₈, a single Mg²⁺ cation per formula unit is randomly distributed between two equivalent positions. At ~ 80 °C, triclinic MgMo₆Se₈ transforms into rhombohedral phase, which is isostructural to the sulfide analogue.²¹ It was also shown^{9,22} that triclinic distortion in MgMo₆Se₈ is associated with a high

Mg mobility and the absence of Mg²⁺ ions' trapping, which takes place in rhombohedral MgMo₆S₈ upon electrochemical Mg extraction.¹⁰

In spite of the previous intensive studies, the phase diagram of the selenide system was not completed because of an extremely high instability of Mg₂Mo₆Se₈.⁹ Thus, the initial aim of this work was to refine the crystal structure of Mg₂Mo₆Se₈ using neutron and synchrotron X-ray diffraction. This refinement resulted in a new and surprising Mg location; thereby our aim was, in addition, to clarify the factors affecting the cation arrangement in CPs by comparative mapping the cation sites for a variety of CPs. This mapping for Mg₂Mo₆Se₈ was also used to confirm the crystal structure's solution, as well as to analyze possible routes of Mg diffusion and finally to explain the high mobility of Mg²⁺ ions in this material.

Experimental Section

The host, Mo₆Se₈, was synthesized by the reaction of a powder of the elements' mixture in an evacuated (10^{-3} Torr) sealed quartz tube (170 h at 1200 °C, followed by quenching in an ice/water bath). The product of the chemical Mg insertion, Mg₂Mo₆Se₈, was obtained via the topotactic reaction of the binary Mo₆Se₈ in contact with a Ph₂Mg/THF solution as the source of Mg²⁺ ions and as the reducing agent.⁹

Synchrotron experiments were carried out in transmission mode at the high-resolution powder diffraction beamline ID31 of the European Synchrotron Radiation Facility (ESRF) in Grenoble, France.²³ Incident X-ray beam with a wavelength of 0.35008(1) Å and 0.4 mm diameter glass capillaries were used to prevent excessive material absorption. The fitting was done in the 2θ -angular range from 1.8 to 35°.

The neutron diffraction experiments were performed at the Institut Laue Langevin at Grenoble, France, on the D1A instrument. A detailed description of this instrument is available via the Internet at <http://www.ill.fr>. D1A is a very high-resolution powder diffractometer operating with the takeoff angle of the monochromator at 122°. In the configuration used, the resolution of D1A was about 0.3° (fwhm) at 90°. The measurements were carried out at a wavelength of $\lambda = 1.911$ Å selected by the (115) reflection of a germanium monochromator. During the neutron diffraction measurements, a cylindrical vanadium sample holder of 7 mm inner diameter was used. The neutron detection was performed with a set of 6° spaced ³He counting tubes. The complete diffraction pattern was obtained by scanning over the whole 2θ range.

The data were analyzed by the Rietveld structure refinement program FULLPROF.^{24,25} Pseudo-Voigt (neutron case) or Thompson–Cox–Hastings pseudo-Voigt functions (synchrotron case) were used for the peak-shape approximation. The background was refined by a polynomial function. The agreement factors used in this article are defined according to the guidelines of the Rietveld refinement that can be found elsewhere.²⁶ The neutron scattering lengths used were $b_{\text{Se}} = 0.7970 \cdot 10^{-14}$ m, $b_{\text{Mg}} = 0.5375 \cdot 10^{-14}$ m, $b_{\text{Mo}} = 0.6715 \cdot 10^{-14}$ m, values taken from ref 27.

(19) Mancour-Billah, A.; Chevrel, R. *J. Solid State Chem.* **2003**, *170*, 281.

(20) McGuire, M. A.; Ranjan, C.; DiSalvo, F. *Inorg. Chem.* **2006**, *45*, 2718.

(21) Levi, E.; Mitelman, A.; Aurbach, D.; Isnard, O. *Inorg. Chem.* **2007**, *46*, 7528.

(22) Levi, M. D.; Lancri, E.; Levi, E.; Gizbar, H.; Gofer, Y.; Aurbach, D. *Solid State Ionics* **2005**, *176*, 1695.

(23) Fitch, A.N. *J. Res. Natl. Inst. Stand. Technol.* **2004**, *109*, 133.

(24) Rietveld, H. M. *J. Appl. Crystallogr.* **1969**, *2*, 65.

(25) Carjaval, J. R. *Physica B* **1993**, *192*, 55.

(26) McCusker, L. B.; Von Dreele, R. B.; Cox, D. E.; Louer, D.; Scardi, P. *J. Appl. Crystallogr.* **1999**, *32*, 36.

(27) Sears, V. F. *Neutron News* **1992**, *3*, 26.

Results and Discussion

Cation Arrangement in CPs and the Factors Affecting This Arrangement. As was mentioned in the Introduction, the crystal structures of CPs differ mostly by cation arrangements, while the coordinates of the anions and the Mo atoms are almost independent of the composition or the symmetry of these compounds.^{1,2} Thus, our first task in the Rietveld analysis was to choose a model of the cation locations for $\text{Mg}_2\text{Mo}_6\text{Se}_8$. For this, it is necessary to analyze the cation arrangement in the known CPs and the factors affecting this arrangement.

It is commonly accepted to illustrate the cation distribution in CPs by three-dimensional presentations of the cavities as distorted cubes with cation positions inside. For instance, Figure 1 compares the relative arrangement of the cation sites in two adjacent cavities 1 and 2 in $\text{Mg}_x\text{Mo}_6\text{S}_8$ for $x = 1$ and 2. However, such a presentation is too general; it cannot reveal the detailed structure of the cavities. Rare maps of the cation sites in CPs, which can be found in the literature, are confined to the relative positions of the inner and outer sites and the distances between them. As a result, such essential information, as the structure of the empty cavities and the structural difference in cavities 2 for triclinic compounds, remained beyond research scope.

In the previous work,⁹ it was shown that mapping of all the cation sites (occupied and vacant) is very useful in the analysis of possible routes for the ionic transport in the CPs' crystal structure. In this paper, we would like to demonstrate that such a mapping could also be very helpful to exhibit the peculiarities of the cation arrangement in different CPs, to follow structural changes related to triclinic distortion, to choose potential models for the Rietveld refinement, and even to verify the validity of structural determinations.

Thus, Figure 2 presents the maps of the cation sites located in a pseudocubic cavity 1 and in three adjacent pseudocubic cavities 2 for CPs' variety (note that the structure of three additional cavities 2 linked to cavity 1 by common faces is not shown in the maps, but it is identical to that of the presented ones, and it can be obtained by inversion in cavity 1's origin). For accurate comparison of the maps, the unit cell parameters of all the CPs are chosen according to increasing angles. The circles on the maps represent the cation sites in the CP's crystal structure, while the numbers inside the circles are the bond valence sums²⁸ (BVS) for these sites. The closer the BVS to the formal electrostatic charge of the cation in ionic compounds, the more suitable is the size of the anion polyhedron for the cation insertion.^{9,29} The occupied sites are marked by blue color (do not forget that this occupation has commonly a random character). Light and dark gray colors were used to distinguish between empty sites suitable and inconvenient for cation intercalation, respectively (a detailed explanation for the sites' mapping based on BVS calculations can be found in ref 29). The maps contain also information about the distances between the adjacent sites. In addition, it takes into account the influence

of the Mo atoms on the sites' potential energy: The sites, which are too close to Mo atoms, are marked by a thick circle line.

Figure 2a–2c shows the evolution of cavities 1 and 2 with Cu insertion into the selenide host, Mo_6Se_8 (the structural data for these maps were taken from refs 1 and 2). According to the map of Figure 2a, the size of the tetrahedral sites in cavity 1 (inner ring) for the host is perfectly convenient for the size of Cu^+ (BVS = 1.01). In contrast, the size of the outer sites is obviously smaller (BVS = 1.55). Taking into account that the outer sites are effectively closer to Mo atoms than the inner ones (3.57 and 2.94 Å, respectively), it is logical to suggest that the potential energy of the latter is lower, and these sites should be occupied at the first stage of Cu insertion.

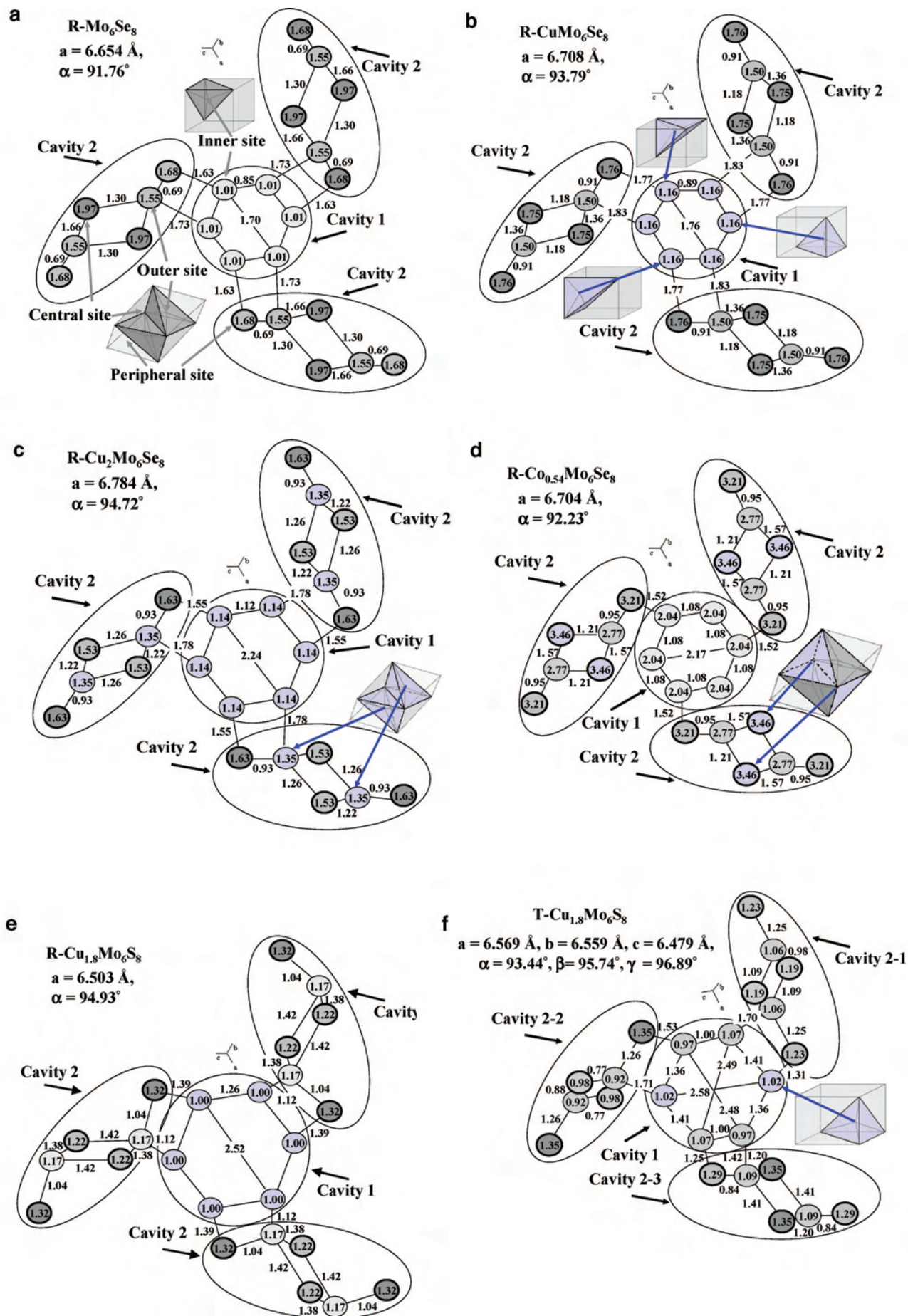
In fact, the cation distributions in $\text{Cu}_x\text{Mo}_6\text{Se}_8$, for $x = 1$ and 2 (Figure 2b and c, respectively) demonstrate a successive occupation of the inner ring for $x = 1$ and the inner plus outer rings for $x = 2$ (note that the inner ring in CuMo_6Se_8 with its maximal distance of 1.76 Å between the sites is convenient for insertion of only one cation per formula unit). The additional tetrahedral sites in cavity 2, which can be defined as central and peripheral sites, are essentially smaller (BVS = 1.97 and 1.68, respectively, for Mo_6Se_8) and closer to Mo atoms (2.37 and 2.53 Å, respectively, for Mo_6Se_8) (a polyhedral linkage in cavities 1 and 2 was presented in ref 9). As a result, these sites remain empty.

The CuMo_6Se_8 example shows that basically the energy of the cation sites and the corresponding cation distribution can be predicted by the sites' geometry of the host and should be similar for all CPs with "small" cations. Actually, in our previous work¹⁰ devoted to the crystal structure of rhombohedral $\text{Mg}_x\text{Mo}_6\text{S}_8$ ($x = 1$ and 2), our models for the Rietveld analysis were based on the successive occupation of the inner and outer sites, and these models were confirmed in the experiments. However, a careful comparison between Figure 2a–2c shows also that the structure of the cavities (the sites' dimensions and the distances between them), especially that of cavity 2, depends on the intercalation level (see, e.g., the BVS of the central sites in cavity 2, which decreases from 1.97 for Mo_6Se_8 to 1.53 for $\text{Cu}_2\text{Mo}_6\text{Se}_8$). It means that the energy of the cation sites in the CPs is not constant but changes with cation insertion. As a result, such simple predictions may not realized in practice, in particular, in the case when additional factors influence the sites' energy.

An example of such a deviation from the classic scheme is the crystal structure of the transition metals' selenides, where the metal–metal interactions between the inserted cations and the Mo atoms change the cation distribution.^{17–19} Figure 2d presents a map of the cation sites for rhombohedral $\text{Co}_{0.54}\text{Mo}_6\text{Se}_8$ (this map was depicted based on structural data of ref 19). As can be seen, the Co cations are located exclusively in the central sites of cavity 2 with short Co–Mo distances (2.50 Å) (the formal oxidation state of Co in this compound is about +3.5). Interestingly, in contrast to $\text{Cu}_x\text{Mo}_6\text{Se}_8$, the empty sites in this compound are effectively larger than the occupied sites. It means that Co cations draw together the adjacent selenium anions.

(28) Brese, N. E.; O'Keefe, M. *Acta Crystallogr.* **1991**, *B47*, 192.

(29) Brown, I. D. *Acta Crystallogr.* **1992**, *B48*, 553.



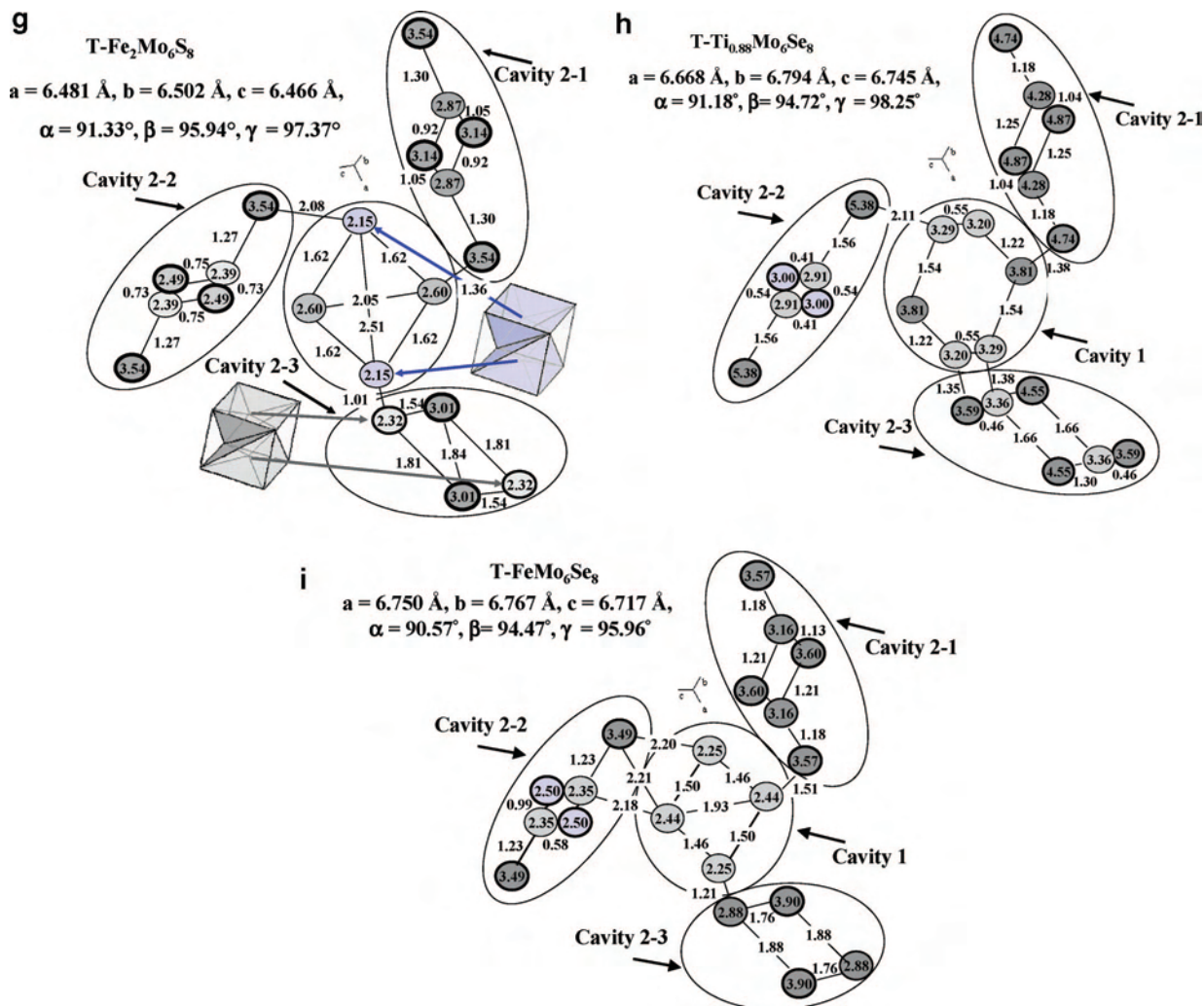


Figure 2. Maps of the cation sites for a variety of CPs. The projections are normal to (ex) -3 symmetric axis. The CP type is indicated on the upper right part of each map. The notations R and T refer to the rhombohedral and triclinic forms, respectively. The insets show the arrangement of the coordination polyhedra in cavities 1 and 2. The occupied sites are colored by blue.

Another example of the factors that can change the site's energy is the metal–metal interactions between the inserted cations. For instance, for $\text{Cu}_x\text{Mo}_6\text{S}_8$ ($x \geq 1.8$) (Figure 2e; structural data of ref 12), instead of the expected arrangement of “one cation in the inner ring + one cation in the outer ring”, two Cu^+ cations are located in the inner ring, forming a Cu–Cu pair with very short interatomic distance (2.52 Å). The random position of the pair within the inner ring results in rhombohedral symmetry of the crystals at room temperature. On cooling, the structure contraction leads to an inner ring with a smaller radius. The matching between the dimensions of the Cu–Cu pair and the ring can be ensured only by the deformation of the latter,²¹ associated with the fixed position of the pairs in the T-form (Figure 2f; structural data of ref 13).

In general, the higher flexibility of the triclinic framework as compared to the rhombohedral allows for relaxation of different structural strains arising between the host and the inserting cations.²¹ For instance, in $\text{T-Fe}_2\text{Mo}_6\text{S}_8$ (Figure 2g; structural data of ref 14), the triclinic structure ensures not only formation of the Fe–Fe pairs but also a more symmetric cation environment with higher CN (CN = 5).¹⁴ A com-

parison between Figure 2f and g demonstrates that, in $\text{T-Fe}_2\text{Mo}_6\text{S}_8$, the distortion of the rhombohedral CPs' framework is essentially higher. In fact, in the latter compound, the hexagonal inner ring of cavity 1 and the six sites of cavity 2-3, which are typical for R-CPs with “small” cations, transform into a combination of four sites (two tetrahedra and two square pyramids⁹) in each cavity. The polyhedral linkage of cavities 2-1 and 2-2 for $\text{T-Fe}_2\text{Mo}_6\text{S}_8$ is similar to that of the R-forms, but variations in the tetrahedra's dimensions of the outer and central sites in these cavities are quite significant. These maps illustrate also very clearly a difference in the orientation of the Fe–Fe and Cu–Cu pairs.¹⁴ In $\text{Cu}_{1.8}\text{Mo}_6\text{S}_8$, the occupied sites in cavity 1 are close to those of cavity 2-1, while in $\text{Fe}_2\text{Mo}_6\text{S}_8$, they are close to cavity 2-3. It seems that the reason for this difference is steric factor, which is very important for CPs,^{1,2,21} in addition to the more covalent character of the Cu–S bonds (CN = 4), as compared to the Fe–S ones (CN = 5).

Similar features related to triclinic distortion can be found in the maps of $\text{T-Ti}_{0.88}\text{Mo}_6\text{Se}_8$ and $\text{T-FeMo}_6\text{Se}_8$ (Figure 2h,i; structural data of ref 19), but in these compounds, the cations are located in the central sites of cavity 2-2, testifying for

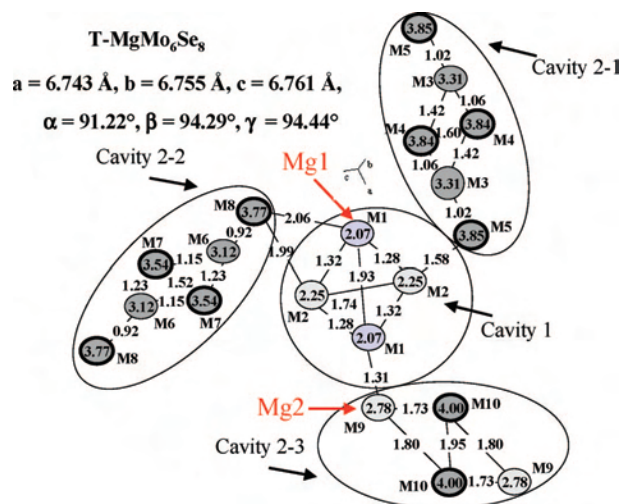


Figure 3. A map of the cation sites for T-MgMo₆Se₈.

the metal–metal interactions between the intercalating ions and the Mo atoms.¹⁹ According to literature data,¹⁹ the materials' crystal structures differ only by the values of the cation shift from the origin of cavity 2. However, the maps demonstrate additional details, such as the distinctions in the distortion of the inner rings. In spite of the different cation location, the polyhedral linkage of T-FeMo₆Se₈ is similar to that of T-Fe₂Mo₆Se₈. In contrast, the structure of the cavities in T-Ti_{0.88}Mo₆Se₈ is closer to that of T-Cu_{1.8}Mo₆Se₈. A comparison of these maps with that of R-Co_{0.54}Mo₆Se₈ reveals a fundamental difference in the distributions of the cation charge in these compounds, which is homogeneous for the R-form and inhomogeneous for the T-form. Actually, for all the triclinic compounds discussed above, the structure of the three cavities 2 is obviously different, but for Ti_{0.88}Mo₆Se₈ and T-FeMo₆Se₈, the anisotropy of the CPs' structure is the highest because the cations are located only in one of cavities 2, that is, only in one of the three channels, which penetrate the Mo₆T₈ framework (note that, in contrast to cavities 2, cavity 1 is common for all three channels, which are equivalent for the R-forms).

Rietveld Analysis for the Mg₂Mo₆Se₈. According to the analysis of the main structural types of CPs performed above, it is logical to suggest that the crystal structure of Mg₂Mo₆Se₈ should follow the classical scheme of a successive occupation of the inner and outer sites. Actually, in this case, the existence of the metal–metal interactions seems to be impossible due to dominant cation repulsion. It means that Mg₂Mo₆Se₈ should “inherit” the cation arrangement of MgMo₆Se₈, and the crystal structure of the latter can be used as a starting setup in the refinement procedure. Thus, our task would only be to choose the position available for the second Mg²⁺ cation in this structure.

Figure 3 shows the map of all the cation sites in the crystal structure of MgMo₆Se₈ obtained in the previous work.⁹ As can be seen, cavity 1 in MgMo₆Se₈ provides four cation sites: two M1 sites with a square-pyramidal coordination (CN = 5) and two M2 sites with a tetrahedral coordination (CN = 4). Thus, the structure is very similar to that of T-Fe₂Mo₆Se₈,¹⁴ but, in contrast to the latter, cavity 1 is able

to accept only one Mg²⁺ cation. In fact, the maximal distance between the cation sites of the inner ring in MgMo₆Se₈ (M1–M1) is equal to ~1.93 Å. According to the BVS values, both the positions, M1 and M2, in cavity 1 are convenient for the insertion of the first Mg²⁺ cation. However, the Rietveld analysis in the previous work⁹ showed that the cations in MgMo₆Se₈ are located only in the M1 sites; thereby this position was chosen for the first Mg atom as the starting one (this example, as well as the maps for other CPs such as R- and T-Cu_{1.8}Mo₆Se₈, demonstrates that a suitable geometry of the cation sites, evident by their BVS values, is necessary but not sufficient condition for these sites to be occupied).

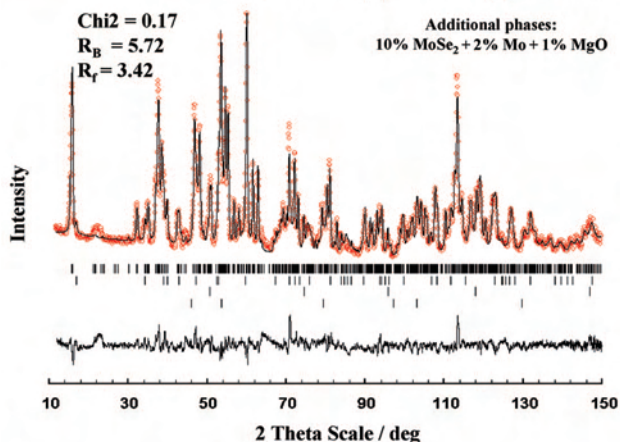
On the basis of the map, it can be suggested that the most appropriate location for the second Mg²⁺ cation is the M9 site (CN = 5) in cavity 2-3 with BVS = 2.78. In fact, the outer tetrahedral sites in cavities 2-1 and 2-2 (M3 and M6, respectively) are distinctly smaller (BVS = 3.31 and 3.12, respectively). In addition, the higher CN should have some energetic advantage. Thus, our initial structural model was based on the combination of the M1 and M9 sites for the first and the second Mg atoms, respectively. Possible simultaneous occupation of these sites by two Mg²⁺ cations in Mg₂Mo₆Se₈ is marked by red arrows in Figure 3 (note that the adjacent M1 and M9 sites are too close to each other to be simultaneously occupied; the distance between them is only 1.31 Å, while the distance between the marked sites is quite appropriate, about 3 Å for MgMo₆Se₈ and about 4 Å for Mg₂Mo₆Se₈).

The refinement performed for this model confirmed a triclinic symmetry for Mg₂Mo₆Se₈ but resulted in relatively high *R* factors, for example, *R*_B = 8.46 (for this refinement, we used the neutron diffraction pattern as the most sensitive to the positions of the light Mg atoms). These *R* factors can be slightly improved by the refinement of the atomic thermal parameters for Mo and Se and by their reasonable increase for Mg. Thus, the initial values (0.33 Å² for Mo, 0.5 Å² for Se, and 1 Å² for Mg) chosen according to the literature data¹⁹ and used in the previous work⁹ for MgMo₆Se₈ were changed to 0.89 Å² for Mo, 1.13 Å² for Se, and 2.5 Å² for Mg (see similar values of these parameters in ref 18). However, the fitting improvement was not significant (e.g., *R*_B = 7.81).

Attempts to refine the structural parameters of Mg in the M1 site led to unreasonable coordinates (too close to Se atoms) and to the decrease of the site occupancy from 0.5 to 0.15 (note that, for this position in the crystal structure, the occupancy of 0.5 corresponds to one atom per formula unit). Similar results were obtained for a model with a location of the first and the second Mg atoms in the M2 and M9 sites, respectively. Thus, the Rietveld analysis showed that the presence of Mg in cavity 1 is improbable; that is, Mg₂Mo₆Se₈ does not follow the classical scheme, and its crystal structure is not similar to that of MgMo₆Se₈.

An alternative option is the location of both the Mg²⁺ ions only in cavities 2. Actually, in contrast to the inner ring of sites, which can adopt only one cation like Li⁺ or Mg²⁺, the dimension of the outer ring is large enough to allow for the simultaneous occupation of three of the six

a $\text{Mg}_2\text{Mo}_6\text{Se}_8$ P -1 (2) $a = 6.878 \text{ \AA}$, $b = 6.930 \text{ \AA}$, $c = 6.888 \text{ \AA}$
 $\alpha = 93.03^\circ$, $\beta = 94.37^\circ$, $\gamma = 96.23^\circ$



b $\text{Mg}_2\text{Mo}_6\text{Se}_8$ P -1 (2) $a = 6.868 \text{ \AA}$, $b = 6.921 \text{ \AA}$, $c = 6.880 \text{ \AA}$
 $\alpha = 93.00^\circ$, $\beta = 94.40^\circ$, $\gamma = 96.22^\circ$

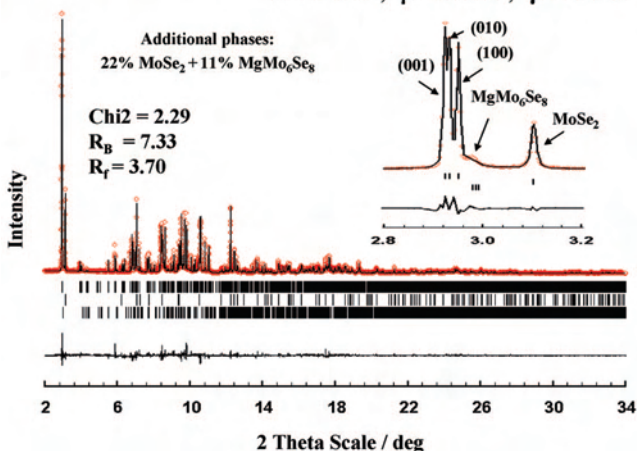


Figure 4. Rietveld profiles for T- $\text{Mg}_2\text{Mo}_6\text{Se}_8$ (27 °C): (a) neutron diffraction, (b) X-ray synchrotron diffraction. The calculated 2θ values of the reflections (vertical bars) correspond to (a) $\text{Mg}_2\text{Mo}_6\text{Se}_8$, MoSe_2 , Mo , and MgO ; (b) $\text{Mg}_2\text{Mo}_6\text{Se}_8$, MoSe_2 , and MgMo_6Se_8 (top-down).

sites by these ions. For instance, in $\text{Li}_4\text{Mo}_6\text{S}_8$, in addition to one Li in the inner ring, three Li^+ cations are distributed in the outer ring,³⁰ thus diminishing the strong repulsion between inserted Li^+ cations. Moreover, ab initio calculations performed in a previous work¹⁰ for $\text{Mg}_2\text{Mo}_6\text{S}_8$ at zero temperature predicted the arrangement of both the Mg atoms per formula unit in the outer sites as the most stable one. As was shown,¹⁰ this prediction is not realized for the rhombohedral modification of $\text{Mg}_2\text{Mo}_6\text{S}_8$ existing at ambient conditions, but it appears to be relevant for triclinic $\text{Mg}_2\text{Mo}_6\text{Se}_8$. Thus, our new model was based on the uniform Mg distribution between all the outer sites, M3, M6, and M9.

Figure 4 presents the results of the Rietveld refinement based on this model. The diffraction profiles shown in Figure 4a,b were obtained for $\text{Mg}_2\text{Mo}_6\text{Se}_8$ with neutron and X-ray synchrotron sources, respectively. It seems that the material prepared for the neutron experiment was not dry enough because, according to the fitting with various cation arrange-

ments, a broad peak around $20^\circ/2\theta$ on the neutron scan is not related to the phase under study but rather to some organic impurity. In spite of the presence of this and other impurities (10% MoSe_2 , 2% Mo , and 1% MgO), the major aim of the synthesis was reached: The sample used for the neutron diffraction studies did not contain a visible amount of triclinic MgMo_6Se_8 (product of material decomposition). As a result, the neutron profile obtained in the experiment was sensitive enough to the positions of the Mg atoms. In fact, the pattern includes 751 reflections of the phase under study. The numbers of the reflections related to the impurities are as follows: 42 for MoSe_2 , 5 for Mo , and 7 for MgO . Taking into account the high resolution of the diffraction peaks and the relatively small amount of the impurities, it is clear that the influence of the latter on the analysis quality is negligible. This conclusion is confirmed by the low values of R factors obtained in the refinement: $\chi_2 = 0.17$, $R_B = 5.72$, $R_f = 3.42$.

The sample studied by the X-ray diffraction contained about 22% of layered MoSe_2 (due to nonoptimal synthetic conditions). The stacking faults existing in the latter material have strong influence on its diffraction peaks, whereas it is difficult to take them into account within the Fullprof program. In addition, our experience³¹ shows that the synchrotron diffraction profile of Mg-containing CPs is strongly affected by compositional gradients. Actually, in spite of the sample storage in the closed glass capillary, the unstable $\text{Mg}_2\text{Mo}_6\text{Se}_8$ loses partly its Mg due to reaction with oxygen traces. This loss results in the formation of MgMo_6Se_8 and MgO (in small amount) accompanied by nonuniform Mg distribution in the CPs crystal structure (The Mg mass-balance is presented in the previous work⁹). Such unhomogeneity caused by compositional gradient can be successfully treated in the Fullprof program as apparent strain in the case of rhombohedral CPs, but this method seems to be less effective for triclinic phases.

These features result in relatively high R factors for the synchrotron profile. In addition, they lead to some difference in the data obtained by the two refinements. Nevertheless, both of the fittings have a similar solution for the $\text{Mg}_2\text{Mo}_6\text{Se}_8$ crystal structure: space group $P\bar{1}$, $a = 6.868 \text{ \AA}$, $b = 6.921 \text{ \AA}$, $c = 6.880 \text{ \AA}$, $\alpha = 93.00^\circ$, $\beta = 94.40^\circ$, $\gamma = 96.22^\circ$. Here the unit cell parameters correspond to the X-ray data. The nonstandard triclinic unit cell for $\text{Mg}_2\text{Mo}_6\text{Se}_8$, with the increasing angles, was chosen for easier comparison with the MgMo_6Se_8 crystal structure (for the latter, $a = 6.743 \text{ \AA}$, $b = 6.755 \text{ \AA}$, $c = 6.761 \text{ \AA}$, $\alpha = 91.22^\circ$, $\beta = 94.29^\circ$, $\gamma = 94.44^\circ$).

Table 1 lists the atomic positions (with standard deviations indicated in parentheses) in the crystal structure of $\text{Mg}_2\text{Mo}_6\text{Se}_8$. Here the upper and the lower values are related to the neutron and synchrotron data, respectively. As can be seen, the refinements confirm the location of Mg^{2+} ions in all the three cavities 2, but their occupancy is effectively different. Similar to $\text{Mg}_2\text{Mo}_6\text{Se}_8$, the sites in cavity 2-3 are the most convenient for Mg^{2+} ions' insertion, while the sites

(30) Ritter, C.; Gocke, E.; Fischer, C.; Schollhorn, R. *J. Mater. Res. Bull.* **1992**, *27*, 1217.

(31) Levi, E.; Mitelman, A.; Aurbach, D.; Brunelli, M. *Chem. Mater.* **2007**, *19*, 5131.

Table 1. The Atomic Coordinates in the Crystal Structure of $\text{Mg}_2\text{Mo}_6\text{Se}_8$ (The Corresponding Standard Deviations Are Given in Parentheses; the Upper and the Lower Values Refer to the Neutron and the Synchrotron Data, Respectively)

atom	site	cavity	X	Y	Z	occ.
Mo1	2i		0.2343(12)	0.4193(11)	0.5479(13)	1
			0.2382(5)	0.4154(5)	0.5480(5)	
Mo2	2i		0.4147(12)	0.5418(12)	0.2379(13)	1
			0.4174(5)	0.5449(5)	0.2420(6)	
Mo3	2i		0.5383(12)	0.2419(13)	0.4119(12)	1
			0.5437(5)	0.2407(5)	0.4179(5)	
Se ₁	2i		0.1270(9)	0.7100(9)	0.3687(8)	1
			0.1257(5)	0.7115(5)	0.3636(5)	
Se ₂	2i		0.3622(10)	0.1172(10)	0.7225(10)	1
			0.3596(5)	0.1174(5)	0.7179(5)	
Se ₃	2i		0.7011(8)	0.3804(8)	0.1320(10)	1
			0.7036(5)	0.3751(5)	0.1263(6)	
Se ₄	2i		0.2088(10)	0.2107(9)	0.2192(9)	1
			0.2048(5)	0.2116(5)	0.2202(5)	
Mg1	2i - M3	2-1	0.020(1)	0.395(1)	0.954(1)	0.24(2)
			0.022(1)	0.398(1)	0.975(1)	0.23(1)
Mg2	2i - M6	2-2	-0.004(4)	-0.021(2)	0.550(4)	0.30(2)
			0.018(2)	-0.015(2)	0.557(3)	0.22(1)
Mg3	2i - M9	2-3	0.349(3)	0.943(2)	0.040(3)	0.46(2)
			0.352(2)	0.953(2)	0.046(1)	0.30(1)

Table 2. The Interatomic Distances (Å) and the Bond Valence Sum (BVS) for the Cations in $\text{Mg}_2\text{Mo}_6\text{Se}_8$

distance	$\text{Mg}_2\text{Mo}_6\text{Se}_8$	BVS
Mo-Mo	2.640(12); 2.665(12); 2.681(13); 2.711(12); 2.738(12); 2.750(12); 3.552(12)	
Mo-Se	2.486(10); 2.505(10); 2.520(10); 2.526(11); 2.554(10); 2.564(10); 2.598(11); 2.605(11); 2.635(10); 2.664(10); 2.664(11); 2.666(11); 2.675(11); 2.710(11); 2.782(11)	
Mo-Mg1	3.18(1); 3.31(1); 3.39(1)	
Mo-Mg2	3.04(2); 3.31(2); 3.70(3)	
Mo-Mg3	3.22(1); 3.30(2); 3.48(2)	
Mg1-Mg1	1.54(1)	
Mg2-Mg2	0.77(4)	
Mg3-Mg3	2.26(3)	
Mg1-Se	2.51(1); 2.52(1); 2.53(1); 2.54(1); 3.57(1)	2.30
Mg2-Se	2.45(2); 2.48(2); 2.53(3); 2.75(3); 2.97(3)	2.24
Mg3-Se	2.46(2); 2.49(2); 2.56(2); 2.56(2); 3.66(2)	2.26
Se-Se	3.72 (3.568 \pm 3.848 \pm 0.011) the mean value of the 18 shortest distances	

in cavities 2-1 and 2-2 are less suitable (for this comparison, we kept the site notation of MgMo_6Se_8).

The data in Table 1 related to neutron diffraction were used to calculate the interatomic distances with their standard deviations, as well as the BVS values (Table 2). As can be seen, the distances, obtained by the refinement, are consistent. They confirm the stability of the rigid structure for the Mo_6Se_8 cluster, despite the additional degree of freedom in the atomic coordinates caused by the triclinic distortion. According to the Mg-Se distances and the BVS values, the coordination of all the inserted Mg^{2+} ions is tetrahedral. It means that, in contrast to MgMo_6Se_8 , the crystal structure of $\text{Mg}_2\text{Mo}_6\text{Se}_8$ cannot be related to the $\text{Fe}_2\text{Mo}_6\text{S}_8$ -type. The polyhedral linkage of all the cation sites, including the vacant ones, for $\text{Mg}_2\text{Mo}_6\text{Se}_8$, is similar to that of triclinic, low-temperature $\text{Cu}_{1.8}\text{Mo}_6\text{Se}_8$, but the occupation of these sites is different because the latter compound can be regarded as a classic CP with preferential location of Cu^+ ions in cavity 1.¹³ Thus, $\text{Mg}_2\text{Mo}_6\text{Se}_8$ presents a new type of cation arrangement in CPs.

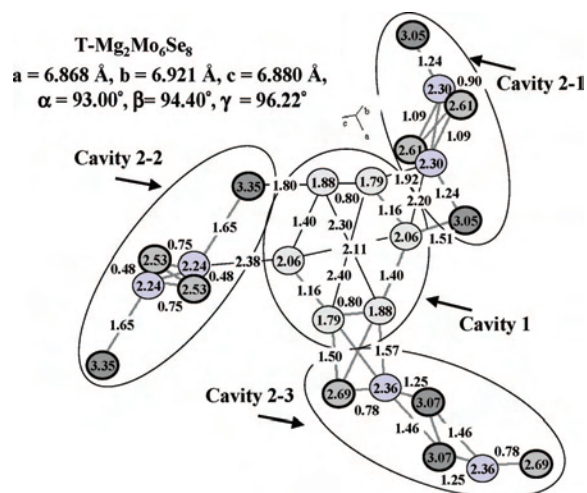


Figure 5. A map of the cations sites for $\text{T-Mg}_2\text{Mo}_6\text{Se}_8$.

Confirmation of the Crystal Structure Solution by the BVS Mapping. As was shown in the previous part, the solution obtained by the Rietveld refinement was surprising: In contrast to that of the sulfides, the crystal structure of $\text{Mg}_2\text{Mo}_6\text{Se}_8$ does not inherit the cation location of MgMo_6Se_8 . Hence, instead of the expected classic intercalation scheme of one cation in the inner ring and another in the outer ring, both cations are distributed between three different cavities 2. Thus, special efforts should be done to confirm the solution, as well as to clarify the factors, which stabilize such unusual cation distribution in CPs.

The validity of the cation arrangement in $\text{Mg}_2\text{Mo}_6\text{Se}_8$ can be verified by analyzing the map of all the cation sites in this crystal structure (Figure 5), as well as by its comparison with similar maps for MgMo_6Se_8 (Figure 3) and other CPs (Figure 2). The cation insertion into M1 and M9 sites, which was assumed by the classic scheme, should retain the polyhedral linkage of the cavities typical for MgMo_6Se_8 , namely, two square pyramids and two tetrahedra in each of the cavities 1 and 2-3. Moreover, the location of both Mg^{2+} cations exclusively in one of the three channels should increase the expansion of the structure in this direction and the difference in three cavities 2. However, this is not the case.

As can be seen by comparison of Figures 3 and 5, the expansion of all cavities 2 for $\text{Mg}_2\text{Mo}_6\text{Se}_8$ is relatively uniform: The BVS values, equal to 3.31, 3.12, and 2.78 for the outer sites in cavities 2-1, 2-2, and 2-3, respectively, for MgMo_6Se_8 decrease to 2.30, 2.24, and 2.36 for $\text{Mg}_2\text{Mo}_6\text{Se}_8$. Moreover, the insertion of the second cation results in the structural type change: Instead of the four cation sites (two square pyramids and two tetrahedra⁹) typical for MgMo_6Se_8 , cavity 1 in $\text{Mg}_2\text{Mo}_6\text{Se}_8$ provides six tetrahedral sites like in the rhombohedral forms. Thus, the analysis of the $\text{Mg}_2\text{Mo}_6\text{Se}_8$ map confirms the results of the Rietveld refinement by revealing a uniform expansion of the cavities' structure in all directions normal to the ex-3-fold symmetry axis. This expansion is related to the homogeneous distribution of the cation charge in this compound, in spite of its triclinic symmetry. Such a distribution should be associated with clear energetic advantage, and it

seems to be a rational reason for the shift of both the Mg^{2+} cations to the outer sites. Hence, a classic scheme, in which CPs with high intercalation level inherit the cation location of the previous level, should be relevant rather to rhombohedral compounds (with a priori uniform distribution of the cation charge), but not to the triclinic ones, especially in the case of multivalent cations' insertion.

The map in Figure 5 illustrates also very clearly the origin of the exceptionally high mobility of Mg^{2+} ions in $\text{Mg}_2\text{Mo}_6\text{Se}_8$: The crystal structure of this compound includes a large number of closely located vacant sites, which are completely convenient for Mg ions transport (see, for instance, the BVS of the inner sites of cavity 1).

Conclusion

A combination of neutron and high-resolution synchrotron X-ray diffractions was used to study the crystal structure of $\text{Mg}_2\text{Mo}_6\text{Se}_8$, which is triclinic at room temperature (space group $P\bar{1}$, $a = 6.868 \text{ \AA}$, $b = 6.921 \text{ \AA}$, $c = 6.880 \text{ \AA}$, $\alpha = 93.00^\circ$, $\beta = 94.40^\circ$, $\gamma = 96.22^\circ$). This structure differs from other members of the $\text{Mg}_x\text{Mo}_6\text{T}_8$ ($x = 1$ and 2 , $T = \text{S, Se}$) family: The rhombohedral sulfide analogues and triclinic MgMo_6Se_8 can be described as classic CPs with preferential cation occupancy of cavity 1, while in $\text{Mg}_2\text{Mo}_6\text{Se}_8$, as in the CPs' selenides of the transition metals, all the cations are located only in cavities 2. However, the Mg^{2+} ions' location in the classic sites of the outer ring is quite different from that of transition metal cations. Hence, triclinic $\text{Mg}_2\text{Mo}_6\text{Se}_8$ presents a new type of cation arrangement in

CPs. A mapping of all the cation sites in this and other CPs was widely used to follow the structural changes related to triclinic distortion, as well as to analyze the cation distribution for different compounds and the factors affecting this distribution. As was shown, these maps may assist in the selection of the appropriate models for the Rietveld refinement. Moreover, they are also a strong tool for analyzing the validity of the structural determinations. On the basis of this mapping for triclinic $\text{Mg}_2\text{Mo}_6\text{Se}_8$, it can be suggested that a uniform distribution of the cation charge, similar to that of rhombohedral phases, results in stabilization of the crystal structure with unusual cation arrangement. A large number of closely located vacant sites, which are completely convenient for the Mg^{2+} ions' transport, lead to extremely high ionic mobility in $\text{Mg}_2\text{Mo}_6\text{Se}_8$.

Acknowledgment. Partial support for this work was obtained from the Israel–U.S. binational foundation (BSF). The Institut Laue Langevin is warmly acknowledged for providing the neutron facilities. The European Synchrotron Radiation Facility in Grenoble is acknowledged for providing synchrotron radiation facilities. We thank Prof. A. Fitch for his assistance in using the beam-line.

Supporting Information Available: Crystallographic information in the form of a cif file (standard choice of the unit cell). This material is available free of charge via the Internet at <http://pubs.acs.org>.

IC702311F